

# DeepSight: Bridging Depth Maps and Language with a Depth-Driven Multimodal Model

Hao Yang\*

Honbo Zhang\*

hyang@ir.hit.edu.cn

hbzhang@ir.hit.edu.cn

Harbin Institute of Technology

Harbin, China

Yanyan Zhao

Harbin Institute of Technology

Harbin, China

yyzhao@ir.hit.edu.cn

Bing Qin

Harbin Institute of Technology

Harbin, China

qinb@ir.hit.edu.cn

## Abstract

Multimodal large language models (MLLMs) have achieved impressive performance across various tasks such as image captioning and visual question answer (VQA); however, they often struggle to accurately interpret depth information inherent in visual data. In this work, we introduce DeepSight, the first dedicated depth MLLM designed to enhance three-dimensional scene understanding. Unlike conventional methods that align RGB image encodings with text, our approach takes advantage of the unique characteristics of depth images: single-channel grayscale images where the pixel values directly reflect depth cues to improve spatial reasoning. To address challenges associated with limited depth data and the inadequacy of simple channel replication, we construct a novel depth image-text pair dataset and a depth instruction dataset. Depth maps are generated from visual images using the GLPN model, and GPT-4 is employed to curate corresponding depth instructions, an approach validated by LLaVA. Additionally, we modify the ViT encoder in CLIP to incorporate local object information, thereby capturing the subtle continuous variations of depth more effectively. To evaluate the performance of our model, we develop a comprehensive depth question answer benchmark based on existing depth image datasets, which rigorously assesses understanding in typical depth map scenarios. Experimental results demonstrate that DeepSight significantly enhances depth perception and downstream task performance, marking a substantial step forward in multimodal three-dimensional understanding.

## CCS Concepts

- Computing methodologies;

## Keywords

Depth, Multimodal Large Language Model, Stereoscopic Vision

\*Both authors contributed equally to this research.

Permission to make digital or hard copies of all or part of this work for personal or classroom use is granted without fee provided that copies are not made or distributed for profit or commercial advantage and that copies bear this notice and the full citation on the first page. Copyrights for components of this work owned by others than the author(s) must be honored. Abstracting with credit is permitted. To copy otherwise, or republish, to post on servers or to redistribute to lists, requires prior specific permission and/or a fee. Request permissions from [permissions@acm.org](mailto:permissions@acm.org).

Conference acronym 'XX, Woodstock, NY

© 2018 Copyright held by the owner/author(s). Publication rights licensed to ACM.

ACM ISBN 978-1-4503-XXXX-X/2018/06

<https://doi.org/XXXXXXX.XXXXXXX>

## ACM Reference Format:

Hao Yang, Honbo Zhang, Yanyan Zhao, and Bing Qin. 2018. DeepSight: Bridging Depth Maps and Language with a Depth-Driven Multimodal Model. In *Proceedings of Make sure to enter the correct conference title from your rights confirmation email (Conference acronym 'XX)*. ACM, New York, NY, USA, 9 pages. <https://doi.org/XXXXXXX.XXXXXXX>

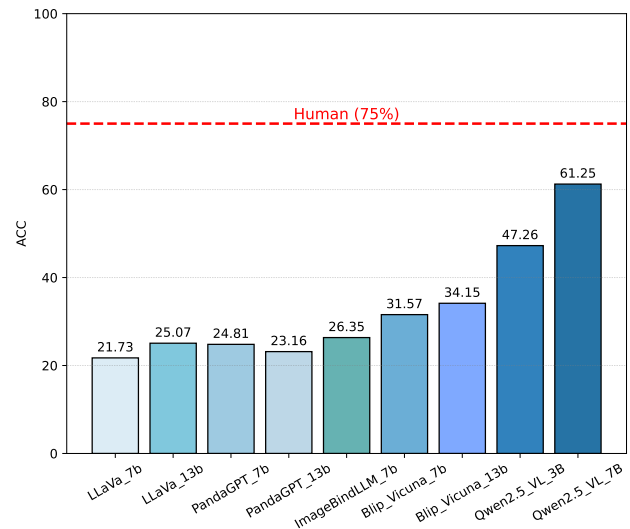


**Figure 1: Stereoscopic Vision Ability Test for MLLMs.** We input RGB images into the MLLMs and ask questions about distance comparisons between objects. The results show that the MLLMs have issues with its stereoscopic vision ability.

## 1 Introduction

Large Language Models (LLMs) have shown remarkable performance on numerous natural language processing tasks [30]. Building on this foundation, Multimodal Large Language Models (MLLMs) further extend this capability to vision-related downstream tasks such as image captioning and image-text retrieval [1, 3, 7, 9, 17, 25], achieving impressive results. However, our experiments reveal that existing MLLMs still struggle to accurately interpret distance information within images.

As illustrated in Figure 1, we conduct a Stereoscopic Vision Ability Test by providing MLLMs only with RGB images and asking them to compare the distances between objects. The results reveal

that MLLMs frequently misjudge which object is closer, highlighting a clear limitation in their spatial understanding. To enable MLLMs to have human-like stereoscopic vision, we believe that incorporating depth information is crucial. Yet, limited data availability and insufficient research on depth-based techniques for MLLMs remain a challenge.

Depth images typically consist of a single grayscale channel whose pixel values explicitly convey spatial distance. Compared with RGB images, depth information can significantly benefit the model’s grasp of three-dimensional structure. By aligning the depth encoding space directly with textual encodings, rather than solely with RGB encoders, MLLMs can achieve a more comprehensive understanding of 3D environments and thus perform better on downstream tasks. Including depth supervision during fine-tuning enables MLLMs to accept depth images as input and yield more accurate results on depth-related downstream tasks.

Previous work such as ImageBind [10] has unified multiple modality encoding spaces by aligning them with RGB image encoders, using only RGB-text pairs for both alignment and instruction tuning. While it offers an initial approach to depth-image comprehension, ImageBind does not fine-tune its depth encoder, thereby limiting the model’s ability to process depth information fully. Hence, constructing dedicated depth image-text pairs and depth instruction data is crucial for enhancing the depth comprehension of such models.

At the same time, to mitigate the scarcity of depth data, we use GLPN [16] to convert RGB images into depth images and employ GPT-4 [15, 33] to generate additional depth instruction data for fine-tuning [23]. Similar approaches have proven effective in previous work like LLaVA [24]. Finally, to systematically evaluate MLLMs’ depth comprehension, we construct a depth question-answering benchmark comprising several sub-tasks based on common depth-related scenarios. This benchmark accurately measures three-dimensional reasoning through a series of template-driven evaluations. In summary, our contributions are as follows:

- We introduce a dedicated benchmark for assessing how well models understand depth information in real-world scenarios. Built on existing depth datasets, this is the first systematic attempt to measure MLLMs’ stereoscopic vision ability through multiple, representative sub-tasks.
- We enhance the ViT within CLIP by incorporating local object information as additional inputs, aiming to improve the model’s capacity to capture fine-grained details and interpret spatial relationships. This adjustment is particularly beneficial for tasks that demand precise depth perception and object interaction.
- We present DeepSight, the first multimodal LLM specifically designed to integrate depth data with text. By incorporating generated depth data in both the alignment and supervised fine-tuning stages, we strengthen the model’s ability to correlate different modalities and refine its understanding of depth images, resulting in more accurate 3D perception.

## 2 Related Work

**Multimodal Large Language Models.** In recent years, multimodal large language models (MLLMs) have made significant progress,

achieving impressive results across a variety of tasks involving both visual and textual understanding. A central theme in this line of work is the alignment between visual encoders and large-scale language models, enabling the unified processing of image-text pairs [18, 19, 21, 34]. For instance, MiniGPT-4 [8, 36] integrates a ViT-based vision encoder with the Vicuna [3, 31] language model through a linear projection layer, demonstrating strong image captioning and reasoning abilities. LLaVA [24] similarly connects the pre-trained CLIP visual encoder (ViT-L/14) to Vicuna and further boosts performance through instruction tuning. In contrast to these direct alignment methods, our approach adopts a two-stage training paradigm: we first optimize the visual and language components independently, then fine-tune them jointly in a task-specific SFT stage. This design improves alignment while preserving the strengths of each modality.

**Depth Images.** Depth images are a specialized form of visual data in which each pixel represents the distance from the camera to surfaces in the scene [6, 12–14]. Unlike standard RGB images that capture texture and color, depth images emphasize geometric structure, often represented as grayscale intensity—closer objects appear brighter, while distant objects are darker. These images are typically obtained via stereo vision, time-of-flight sensors, or structured light, and are widely applied in robotics, 3D reconstruction, and autonomous driving [5]. In computer vision, depth information enhances spatial understanding, enabling more robust object detection, pose estimation, and obstacle avoidance. Despite their value, depth images pose unique challenges due to their lower texture richness and domain differences from natural images. Our work aims to better integrate this underutilized modality into the MLLM paradigm, enhancing multimodal reasoning with 3D-aware representations.

**Scarce-Modality Large Language Models.** While most MLLMs are developed for widely available modalities such as RGB images, audio, and video, less attention has been paid to rare or under-represented modalities like depth, thermal, or radar [20]. Works such as ImageBind [10], LanguageBind [35], and PandaGPT [29] aim to support diverse modalities by projecting them into a shared embedding space. However, these models typically rely on massive heterogeneous datasets and are not specifically optimized for scarce modalities. Our approach diverges by focusing specifically on depth as a primary visual input, and constructing a dedicated depth-text paired dataset for alignment. Through a two-stage training framework—alignment followed by instruction tuning—we achieve efficient learning of depth semantics and effective cross-modal reasoning. This targeted strategy not only reduces resource demands but also improves depth-specific performance in tasks such as distance comparison, object recognition, and spatial reasoning.

## 3 Depth Template Benchmark

Existing evaluation methods for depth modality remain relatively limited and simplistic, with most prior work focusing primarily on scene classification task [4]. However, this narrow scope fails to provide a comprehensive assessment of a model’s capability to understand depth information. One key limitation in the field is the lack of standardized and fine-grained evaluation benchmarks specifically tailored to the depth modality. To address this gap, we

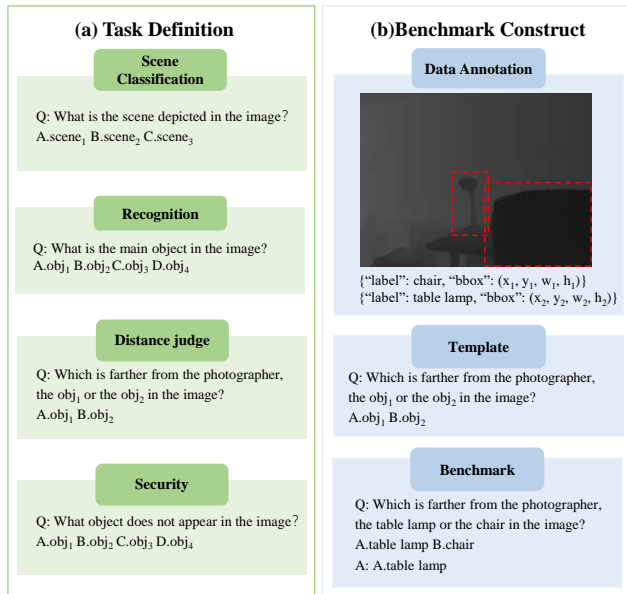


**Figure 2: Benchmark construction. (a) defines the types of tasks. (b) describes how benchmark is constructed from templates.**

propose a depth-based question answering benchmark designed to assess MLLMs’ depth perception and reasoning capabilities [27, 28]. All depth images used in our benchmark are real-world samples containing rich semantic and spatial information, enabling a more thorough and meaningful evaluation of the model’s perceptual understanding. By introducing this benchmark, we aim to establish a more rigorous and targeted evaluation protocol for underexplored modalities like depth.

### 3.1 Task Definition

We define four sub-tasks: Scene Classification, Recognition, Distance Judge, and Security. These tasks are specifically designed to assess both the model’s holistic understanding of the overall scene and its ability to reason about fine-grained, object-level depth cues within depth images. Each task is formulated in a question-answer format, where the model either selects the most suitable answer from a set of candidates or generates a descriptive caption based on visual input.

**Scene Classification.** This task evaluates the model’s global perception by requiring it to classify the entire scene from a depth image. Given three candidate labels, the model must choose the one that best describes the environment. Success in this task reflects an understanding of spatial composition, layout, and contextual depth features that define different scene categories.

**Recognition.** In this task, the model is prompted to identify specific objects located in targeted regions of the depth image. With four candidate answers provided, it must select the label that correctly matches the object. This evaluates the model’s ability to extract meaningful object-level features from geometric cues present in depth data.

**Distance Judge.** This task tests the model’s depth reasoning by asking it to compare the relative distances of two specified objects. Based on region-wise average depth values, the model must determine which object is farther from the viewpoint. This sub-task focuses on the model’s ability to interpret spatial hierarchy and construct a reliable depth-based relational understanding.

**Security.** This task evaluates the model’s ability to judge the completeness of object recognition in a scene. Given four candidate objects, the model is required to identify the one that does not appear in the image. This task focuses on the model’s robustness in maintaining reliable recognition performance under complex scenes and potential category confusion.

### 3.2 Benchmark Construct

As shown in Figure 2, we developed the Depth Template Benchmark by constructing multiple problem templates and utilizing real depth images along with object bounding box annotations. We extract object instance segmentation from the bounding boxes to obtain the precise pixel regions of each object. The average depth within these regions is then utilized to estimate the depth of each object, thereby enabling a relative Distance Judge task among objects.

The distribution of the four sub-task categories is shown in Table 1, with a total of 13,473 question-answer pairs generated.

**Table 1: Task statistics across datasets. We construct four categories of sub-tasks: Scene Classification, Recognition, Distance Judgment, and Security. In total, 13,473 question-answer pairs are generated.**

Task	Source	Count	Percentage (%)
Scene Classification	NYU-D	1,786	13.26
Recognition	SUN-D	3,793	28.15
Distance Judgment	SUN-D	5,737	42.58
Security	SUN-D	2,157	16.01
Total		13,473	100.00

## 4 Depth Instruction Dataset

In this section, we describe the process of constructing the Depth Instruction Dataset. Due to the small scale of real-world depth datasets, which is insufficient for pretraining, we chose to translate RGB images from the COCO [22] dataset into depth images. The dataset construction pipeline consists of three key steps: image translation, caption scoring, and instruction generation. Ultimately, we obtained 118K depth-text-bboxes pairs and 22k depth instructions as shown in Figure 3.

**Image Translation.** We employ the GLPN model to transform RGB images into depth images. The resulting depth images preserve partial semantic information from the original RGB images while gaining enhanced spatial perception, facilitating a more comprehensive understanding of scene geometry. Although the depth information in these generated images is not ground-truth being predicted rather than directly measured our experiments demonstrate that this approach remains highly effective.

Depth image		
Question	Caption the depth image.	What is the interaction between the woman and the dog in the park?
Answer	An adult and young giraffe in an enclosure with people looking at them.	The woman in the park is walking her dog on a leash. The interaction between them suggests a typical scene of a pet owner taking their dog for a walk in a public area like a park. The woman is likely providing guidance and care to ensure the dog's safety and enjoyment during their outing. This demonstrates a common and heartwarming activity between humans and their pets, highlighting the bond and companionship shared between them.

**Figure 3: Sample from the Depth Instruction Dataset. The left side shows a sample of caption data used for alignment, and the right side shows an instruction sample generated by GPT-4.**

**Caption Scoring.** In the COCO dataset, each image is annotated with multiple captions describing diverse scene aspects. However, to enhance the alignment between the image and its corresponding depth representation, we select only the caption that is most relevant to the depth image’s semantics. We use the LanguageBind [26] Depth Encoder to compute similarity scores between each caption and the depth image. By computing similarity scores for all the captions, we identify the highest-scoring caption, ensuring that it is the one most semantically consistent with the depth image. This process helps to filter out captions that may not accurately reflect the depth-related content, ensuring that the chosen caption has a strong semantic match with the depth image. As a result, this approach guarantees a high level of semantic similarity between the depth image and the selected caption. Ultimately, we obtain a total of 118k high-quality depth-text-bboxes pairs, which will be used for subsequent model training.

**Instruction Generation.** We introduce the Depth Instruction Dataset, constructed in a format similar to LLaVA, to improve the alignment between the depth images and textual understanding. The dataset is generated by providing GPT-3.5 with a depth image’s corresponding captions, and object bounding boxes. It is worth noting that for each image, we need to input multiple corresponding captions into GPT-3.5 to ensure that it can understand the image information from various perspectives. Leveraging this data, GPT-3.5 synthesizes instruction-following examples using predefined templates. Ultimately, we obtain three types of instruction data, totaling 22k instances: complex reasoning, multi-round dialogue, and detailed description.

## 5 DeepSight Vision Encoder

In this section, we introduce the vision encoder of DeepSight, a modified version of the original CLIP model that utilizes local object depth information to enhance its understanding of the entire depth image.

### 5.1 Vision Encoder Architecture

The vision encoder introduces structural modifications to the CLIP architecture to enhance its ability to recognize local information, while preserving the model’s existing knowledge. These changes enable the model to better process depth features, which are essential for understanding 3D scenes. At the same time, it retains CLIP’s strength in large-scale text-image pretraining, allowing it to effectively integrate spatial and semantic understanding for tasks that involve both depth and visual comprehension.

As shown in Figure 4, we add a bounding box convolution layer to the ViT architecture for local depth information recognition. Given the depth image  $D$  and the corresponding object bounding box mask  $M$ , the CLIP patch division encoding is applied to both inputs. The encoded depth image  $D$  is processed by the Depth Conv, and the encoded bounding box mask  $M$  is processed by the Bbox Conv. The resulting feature representations are denoted as  $H_D = f(D)$  and  $H_M = g(M)$ , respectively. These two results are then combined and passed into the subsequent attention module, which produces the final vision encoding result  $H_V = H_D + H_M$ . It is important to note that the input to the Bbox Conv is a single-channel matrix, where the values are binary: 0 represents the background and 1 represents the object. The text input  $T$  is directly fed into the CLIP text encoder. The image embedding  $H_V$  and text embedding  $H_T$  are then used to compute a cross-entropy loss, aligning the multimodal representations to ensure coherence between the depth image and the textual description, after applying softmax processing to both embeddings. The cross-entropy formula is expressed as:

$$\mathcal{L}_{CE} = - \sum_{i=1}^N [H_V \log(\hat{H}_T) + H_T \log(\hat{H}_V)]$$

Where  $H_V$  and  $H_T$  are the image and text embeddings after softmax processing, and  $\hat{H}_V$  and  $\hat{H}_T$  are the predicted image and text embeddings.

During inference, depth convolution takes the depth image as input, and the bounding box convolution layer input defaults to 1.

### 5.2 Training Method

During training, we keep the CLIP text encoder frozen and only train the visual encoder. We employ a specific data sampling strategy where depth-box-text pairs are randomly replaced with depth-text pairs. This approach helps preserve the model’s prior knowledge while maintaining its ability to understand the image at a global level. Initially, we set the sample parameter  $r = 0.1$ , randomly replacing depth-box-text pairs with a ratio of  $r$ . At the same time, the input to the bounding box convolution layer is set to 1 for all replacements. During inference, the input to the bounding box convolution layer is likewise set to 1.

## 6 Aligning with LLM

To the best of our knowledge, there are currently no multimodal large language models specifically designed for the depth modality. In this section, we introduce a large language model tailored for depth understanding, leveraging depth encoder and Vicuna alignment to enhance the model’s ability to process depth information [32].

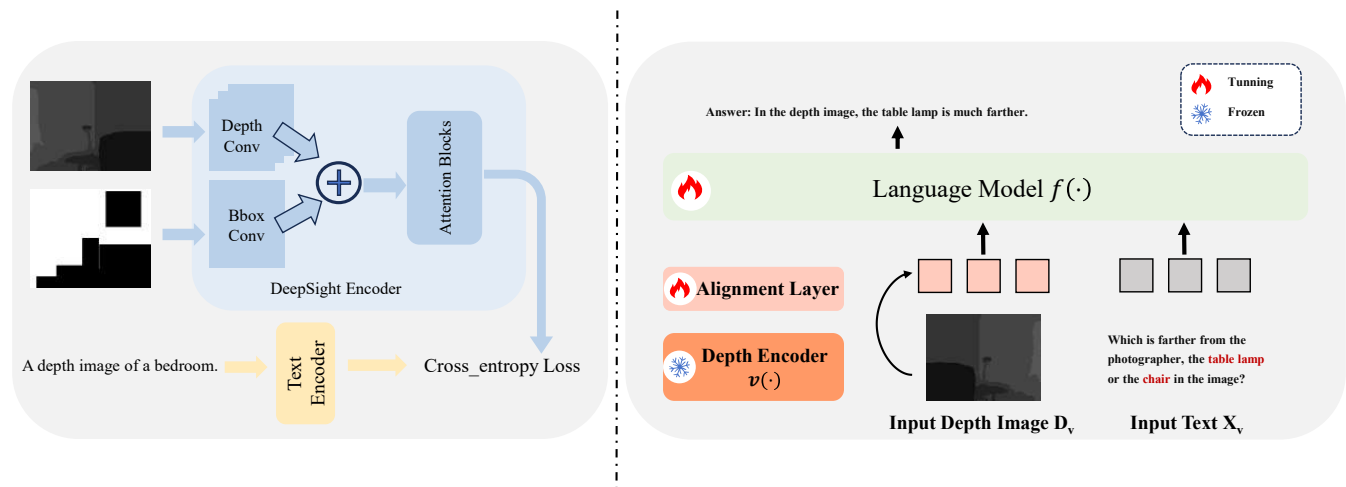


**Figure 4: Overall model architecture.** The left figure shows the Depth Encoder architecture, where DeepSight modifies the CLIP image encoder to take an additional Bbox channel along with depth convolution. The right figure illustrates the model pipeline, showing the data flow from the input question and depth image to the output answer. In the alignment stage, only the Alignment Layer is trained while keeping the Depth Encoder, Text Encoder, and LLM frozen. In the fine-tuning stage, the other modules remain frozen and additional training is performed on the LLM.

## 6.1 Model Architecture

As shown in Figure 4, the DeepSight model consists of three main components: a depth modality encoder, a trainable linear projection layer, and a large language model. Specifically, DeepSight is used as the depth encoder to process depth images, while an MLP (multi-layer perceptron) serves as the alignment layer to correlate the depth information with the text. Vicuna1.5-7B is used as the foundational language model to handle the combined embeddings from both text and depth images. The model takes text and depth images as inputs, aligning the depth features with the text via the MLP, and then merges both modalities’ embeddings. These combined representations are fed into the language model, which generates the appropriate response or output. This architecture enhances the model’s ability to process and interpret multimodal data by integrating depth information with text, allowing for more accurate, context-aware responses that involve complex spatial reasoning and depth perception.

## 6.2 Alignment

Similar to LLaVA, we train the model in two stages to optimize its performance. In the first stage, called the alignment stage, we utilize 118k depth-text pairs from section 4 to train the linear projection layer. The purpose of this phase is to align the DeepSight encoder with the Vicuna1.5-7B model, ensuring that the depth image feature space and the text embedding space are effectively synchronized. This alignment is crucial because it allows the model to process and understand both modalities in a unified manner. During this stage, we freeze both the depth encoder and the large language model, focusing exclusively on training the linear projection layer. By doing so, we isolate the training process, allowing for a more precise adjustment of the mapping between the depth image features and the textual embeddings. This helps to ensure that the depth and

text modalities are properly aligned, which is essential for the model’s ability to handle and interpret both types of data. Once this alignment is achieved, it sets a solid foundation for the subsequent stages of training, where the model can refine its understanding and improve its performance on more complex tasks.

## 6.3 Supervised Fine-tuning

The supervised fine-tuning (SFT) stage is designed to enhance the model’s ability to respond to depth-related instructions, building on the alignment established in the previous stage. During this phase, we leverage a dataset of 22k Depth Instruction Dataset to further train the model. Unlike the alignment stage, where only the linear projection layer was trained, in this stage, we freeze the depth encoder and focus on fine-tuning both the linear projection layer and the large language model. Additionally, we minimize the depth-conditioned text generation loss to ensure the model generates accurate and contextually appropriate responses based on the depth-related instructions. This fine-tuning process allows the model to better handle complex interactions involving depth information, ensuring more accurate and relevant outputs when given depth-specific tasks. By combining the depth instruction data with the previously learned embeddings, the model becomes increasingly adept at processing depth information.

## 7 Experiment

In this section, we conduct comprehensive experiments to evaluate the effectiveness of our proposed DeepSight model. First, we assess the zero-shot scene classification performance of the DeepSight vision encoder, comparing it with a set of strong baseline vision models. Then, we also fine-tune other models using the Depth Instruction dataset and evaluate them on our benchmark.

**Table 2: Performance comparison of depth-aware multimodal models on the Depth Template Benchmark, covering four QA sub-tasks: Scene Classification, Recognition, Distance Judgment, and Security. We evaluate both zero-shot and fine-tuned settings using the Depth Instruction Dataset. LanguageBind is first aligned with Vicuna1.5-7B before fine-tuning. Best results in each column are highlighted in bold.**

Model	Scene Classification	Recognition	Distance Judge	Security	Avg.
<b>(a) Zero Shot</b>					
PandaGPT-7B	28.19	17.15	13.74	43.16	25.56
ImageBindLLM-7B [11]	58.23	23.06	28.74	22.68	33.18
<b>DeepSight-7B (Ours)</b>	57.01	28.72	39.23	29.15	38.53
<b>(b) Fine-tuning</b>					
PandaGPT-7B-FT	36.92	24.38	33.12	44.06	34.62
ImageBindLLM-7B-FT	60.19	27.33	41.82	29.78	39.28
LanguageBind-Aligned-7B-FT	62.31	36.08	57.92	37.84	48.54
<b>DeepSight-7B (Ours)</b>	<b>64.86</b>	<b>40.56</b>	<b>63.17</b>	<b>44.81</b>	<b>53.85</b>

In addition to benchmark comparisons, we also perform ablation studies to investigate the impact of key architectural components. By systematically removing or modifying elements such as the Bbox channel, and alignment layer, we quantify the contribution of each component to the final performance. We also conduct experiments to validate the effectiveness of our constructed Depth Instruction Dataset and the data sample strategy.

These experiments collectively validate the design choices in our model. The results demonstrate that DeepSight not only excels in zero-shot classification tasks but also shows strong generalization to downstream depth-aware question answering tasks, confirming the effectiveness and robustness of our approach.

### 7.1 Zero-shot Scene Classification

We compared our DeepSight vision encoder with other depth-aware visual encoders on the zero-shot scene classification task, and the results demonstrate that our model exhibits state-of-the-art performance. As shown in Table 3, our vision encoder achieves an accuracy of 67.0% and 38.4% on 1,000 randomly selected samples from the NYU-D and SUN-D datasets, respectively, surpassing ImageBind by 13.0% and 3.3%, and LanguageBind by 1.9% and 0.7%. These results demonstrate that the DeepSight depth encoder effectively captures holistic image semantics while exhibiting superior performance in leveraging depth information for scene classification. The substantial improvements over existing models further substantiate the effectiveness of our encoder architecture.

**Table 3: Zero-shot scene classification on 1,000 NYU-D and 1,000 SUN-D images. Our model achieves state-of-the-art accuracy.**

Model	NYU-D (%)	SUN-D (%)
ImageBind	54.0	35.1
LanguageBind	65.1	36.7
<b>DeepSight-7B (Ours)</b>	<b>67.0</b>	<b>38.4</b>

### 7.2 Benchmark Comparison with other Models

To thoroughly evaluate our model’s capacity for understanding depth images, we employ the Depth Template Benchmark, introduced in Section 3, as the primary evaluation framework. This benchmark comprises multiple sub-tasks designed to test different aspects of depth reasoning. All evaluation metrics are based on accuracy to enable fair and interpretable comparisons across models.

We first evaluate several depth-related models on the benchmark in a zero-shot setting, as shown in Table 2(a). Without any fine-tuning, DeepSight achieves the best overall performance with an average score of 38.54%, outperforming PandaGPT-7B with 25.56% and ImageBindLLM-7B with 33.18% in the zero-shot setting. It shows clear advantages in recognition and distance judgment tasks, demonstrating stronger depth understanding ability. It is observed that the DeepSight exhibits lower performance in scene recognition compared to the zero-shot scene classification capability of the depth encoder. This discrepancy can be attributed to the difference in evaluation settings, the current task is framed as a textual question answering task, rather than direct classification.

To ensure a rigorous and fair evaluation, we also fine-tune all baseline models using the Depth Instruction Dataset introduced in Section 4. For consistency, we align the depth encoder of LanguageBind with Vicuna-1.5-7B, which serves as the LLM backbone in our own model. This alignment ensures that differences in performance are attributed to architectural design rather than discrepancies in model scale or backbone capabilities. All models—including PandaGPT\_7B, ImageBindLLM\_7B and the aligned LanguageBind are trained using exactly the same data as our DeepSight model.

As reported in Table 2(b), our model demonstrates consistently superior performance across all four evaluation tasks. It achieves accuracy rates of 64.86% on Scene Classification, 40.56% on Recognition, 63.17% on Distance Judgment, and 44.81% on Security Assessment. These results not only surpass those of all competing baselines but also further substantiate the robustness and generalization capability of our proposed architecture. In addition, both PandaGPT-7B and ImageBindLLM-7B-FT exhibit notable performance improvements after fine-tuning on our Depth Instruction

Dataset, confirming the effectiveness of the constructed instructions in enhancing the depth-related understanding of vision models.

These substantial gains highlight the value of our proposed architecture and the effectiveness of incorporating depth-specific features into the model’s representation learning. The results validate the impact of our generated depth data in significantly enhancing the model’s ability to interpret and reason about depth-aware visual inputs. By leveraging structural and semantic cues uniquely available in depth images—further enhanced through Bbox-guided attention and instruction-aligned training—our model demonstrates strong reasoning capabilities and adaptability to complex multimodal scenarios. Collectively, these findings confirm that our model not only excels on current benchmarks but also establishes a new standard for depth-aware understanding in vision-language systems.

### 7.3 Ablations

We perform a series of ablation studies to better understand the contribution of key design choices in our framework. Specifically, we investigate the effects of the fine-tuning strategy, the inclusion of the Bbox Convolution layer, the use of our instruction dataset, and the data sampling strategy. These experiments are designed to isolate the role of each component and assess how they individually and collectively affect the model’s overall performance.

**SFT Choice.** To verify the importance of fine-tuning the LLM during the SFT stage, we conduct an experiment in which we selectively train either the MLP or the LLM. The Distance Judge task is chosen as the evaluation task for this experiment. In this experiment, we compared the performance of three different training configurations: fine-tuning only the MLP, fine-tuning only the LLM and fine-tuning both the MLP and the LLM together. As shown in Table 5, fine-tuning both the MLP and LLM together resulted in performance improvements of 16.46% and 5.81% compared to training only the MLP or the LLM, respectively. This demonstrates that jointly fine-tuning both the MLP and the LLM during the SFT stage is crucial for maximizing the model’s performance, and highlights the importance of fine-tuning the LLM in conjunction with the alignment layer to fully leverage the depth information in the task. The significant performance gains reinforce the idea that the collaborative training of both components leads to a more effective model.

**Table 4: Ablation study on SFT structure. Ablation study on SFT structure. Results of different configurations evaluated on the Distance Judge sub-task of the Depth Template Benchmark.**

Train MLP	Train LLM	Distance Judge
✓	✗	46.71
✗	✓	57.36
✓	✓	<b>63.17</b>

**Bbox Convolution.** To evaluate the effectiveness of the Bbox Convolution layer in understanding depth information, we conduct an ablation study comparing the performance of distance judgment under different training and inference configurations. As shown

in Table 5, when the Bbox Convolution layer is included during training but excluded during inference, the model achieves a distance judgment accuracy of 58.46%. In contrast, when the Bbox Convolution layer is used during both training and inference, the accuracy improves to 63.17%. These results indicate that retaining the Bbox Convolution layer throughout both stages significantly enhances the model’s ability to reason about depth. This highlights the crucial role of the Bbox Convolution layer in capturing depth-related features and improving performance on distance judgment tasks.

**Table 5: Ablation on the Bbox Convolution. Results of different configurations evaluated on the Distance Judge sub-task of the Depth Template Benchmark.**

Train Bbox Conv	Infer Bbox Conv	Distance Judge
✓	✗	58.46
✓	✓	<b>63.17</b>

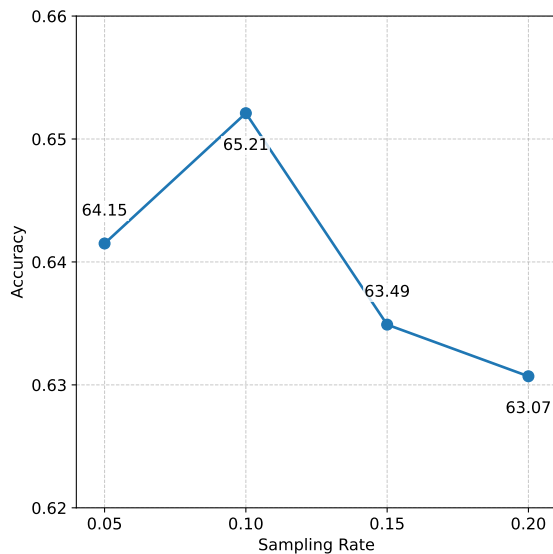
**Data Sample Strategy.** To preserve CLIP’s ability to understand the global structure of depth images, we randomly replace a portion of the depth-text-bboxes pairs with depth-text pairs during training. This strategy allows the model to maintain holistic scene understanding while also acquiring the ability to process localized, object-level information. We use zero-shot Scene Classification top-1 accuracy as the evaluation metric. Specifically, we adopt the ViT-B/16 model and train it on the depth-text-bounding box dataset for 5 epochs. As illustrated in Figure 5, the model without data sampling performs worse than those incorporating sampling. Moreover, we observe that overly high replacement ratios can degrade performance. Based on these observations, we adopt a sample ratio of 0.1 as the optimal setting.

**Instruction Dataset** To validate the effectiveness of our constructed Depth Instruction Dataset in enhancing the stereoscopic perception capabilities of multimodal vision models, we conduct additional fine-tuning on several representative vision-language models and evaluate their performance using the *Depth Template Benchmark*. To ensure compatibility, the depth images are converted to three-channel format and directly used as input across all models, maintaining consistency in training and evaluation settings.

As shown in Table 6, all evaluated models demonstrate significant performance improvements after fine-tuning with our dataset. For example, LLaVA-7B shows an average accuracy gain from 25.69% to 33.81%, while BLIP-Vicuna-7B achieves a substantial boost from 28.20% to 43.91%. Similarly, both variants of QWen2.5-VL benefit from our instruction data, with the 7B model attaining the highest overall performance, increasing from 40.73% to 49.32%. These results not only confirm the value of task-aligned supervision with depth-specific semantics, but also verify that traditional vision-language models, when equipped with explicit depth cues, can better understand the stereoscopic structure and spatial layout of visual scenes.

**Table 6: Performance comparison of general vision-language models on the Depth Template Benchmark, covering four QA sub-tasks: Scene Classification, Recognition, Distance Judgment, and Security. We evaluate both zero-shot and fine-tuned settings using the Depth Instruction Dataset.**

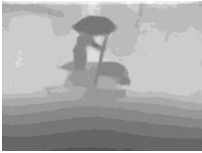
Model	Scene Classification	Recognition	Distance Judge	Security	Avg.
<b>(a) Zero-shot</b>					
LLaVA-7B	30.62	26.15	25.41	20.58	25.69
BLIP-Vicuna-7B	24.17	29.41	30.14	31.07	28.20
QWen2.5-VL-3B [2]	36.83	26.75	31.02	27.58	30.05
QWen2.5-VL-7B	<b>47.59</b>	<b>34.17</b>	<b>46.90</b>	<b>34.25</b>	<b>40.73</b>
<b>(b) Fine-tuning</b>					
LLaVA-7B	41.53	29.71	34.60	27.39	33.81
BLIP-Vicuna-7B	47.25	<b>40.96</b>	49.15	38.26	43.91
QWen2.5-VL-3B	43.16	30.44	42.97	31.17	36.44
QWen2.5-VL-7B	<b>60.62</b>	39.71	<b>58.36</b>	<b>40.60</b>	<b>49.32</b>



**Figure 5: Sample ratio search experiment. We search sample ratio with a step of 0.05. Test metric is zero-shot Scene Classification top-1 accuracy.**

## 8 Case Study

To further assess the effectiveness of our model, we present a case study on representative examples. As shown in Figure 6, DeepSight captures both global scene context and fine-grained object details, demonstrating a balanced understanding of spatial layout and semantics. In contrast, other models show issues such as incorrect object recognition or color description. This comparison highlights how incorporating explicit depth cues improves multimodal models’ fine-grained and context-aware visual understanding, and underscores the value of jointly reasoning over global structure and local details.

	
<b>user</b>	What does this depth image depict?
<b>DeepSight-7B</b>	In the depth image, a group of people are rowing a boat on a river in the rain. At the center, one person is holding a paddle with one hand and an umbrella with the other, while the others stay below him, also holding umbrellas to shield themselves from the rain, with some trees in the background.
<b>PandaGPT_7B</b>	In the image, there is one person standing on the ground, holding a long, stick-like object.
<b>ImageBindLLM_7B</b>	In the image, there is a person walking leisurely in the rain, holding an umbrella.
<b>LanguageBind_Aligned</b>	In this depth map, a person is standing on a boat while others are crouching nearby. It’s raining, and they are all holding umbrellas. The surroundings appear calm and misty, with raindrops gently falling around.

**Figure 6: Case study. We posed questions about the depth image to multiple models, and the results show that DeepSight is better able to meet the task requirements.**

This case study further supports our claim that explicitly incorporating depth information, as done in DeepSight, improves multimodal models’ ability to understand visual scenes both globally and locally. Depth helps the model grasp spatial relationships, object positioning, and occlusions, enabling more precise and context-aware reasoning. It also underscores the importance of designing architectures that can jointly reason about overall scene layout and fine-grained semantics.

## 9 Conclusion

In this paper, we present DeepSight, a depth-modality-specific multimodal large language model designed to enhance the understanding of depth images in multimodal tasks. We first construct the QA Depth Template Benchmark based on real-world datasets to evaluate both global and local depth reasoning. To support model

training, we convert the COCO dataset into depth images, generating 118k depth-text pairs and 22k instruction samples.

We further propose DeepSight, a modified CLIP architecture aligned with large language models through fine-tuning. Finally, ablation experiments validate the effectiveness of both our architectural design and training strategy. Our work highlights the potential of depth-aware multimodal models in advancing stereoscopic visual understanding.

## References

- [1] Jinze Bai, Shuai Bai, Yunfei Chu, Zeyu Cui, Kai Dang, Xiaodong Deng, Yang Fan, Wenbin Ge, Yu Han, Fei Huang, Binyuan Hui, Luo Ji, Mei Li, Junyang Lin, Runji Lin, Dayiheng Liu, Gao Liu, Chengqiang Lu, Keming Lu, Jianxin Ma, Rui Men, Xingzhang Ren, Xuancheng Ren, Chuanqi Tan, Sinan Tan, Jianhong Tu, Peng Wang, Shijie Wang, Wei Wang, Shengguang Wu, Benfeng Xu, Jin Xu, An Yang, Hao Yang, Jian Yang, Shusheng Yang, Yang Yao, Bowen Yu, Hongyi Yuan, Zheng Yuan, Jianwei Zhang, Xingxuan Zhang, Yichang Zhang, Zhenru Zhang, Chang Zhou, Jingren Zhou, Xiaohuan Zhou, and Tianhang Zhu. 2023. Qwen Technical Report. arXiv:2309.16609 [cs.CL] <https://arxiv.org/abs/2309.16609>
- [2] Shuai Bai, Keqin Chen, Xuejing Liu, Jialin Wang, Wenbin Ge, Sibao Song, Kai Dang, Peng Wang, Shijie Wang, Jun Tang, et al. 2025. Qwen2. 5-vl technical report. arXiv preprint arXiv:2502.13923 (2025).
- [3] UC Berkeley, Stanford Cmu, and UC San. [n. d.]. Vicuna: An Open-Source Chatbot Impressing GPT-4 with 90% ChatGPT Quality. ([n. d.]).
- [4] Matthew Brown and Sabine Süsstrunk. 2011. Multi-spectral SIFT for scene category recognition. In *CVPR 2011*. IEEE, 177–184.
- [5] Wenxiao Cai, Iaroslav Ponomarenko, Jianhao Yuan, Xiaoqi Li, Wankou Yang, Hao Dong, and Bo Zhao. 2024. Spatialbot: Precise spatial understanding with vision language models. arXiv preprint arXiv:2406.13642 (2024).
- [6] Yuanzhouhan Cao, Zifeng Wu, and Chunhua Shen. 2018. Estimating Depth from Monocular Images as Classification Using Deep Fully Convolutional Residual Networks. *IEEE Transactions on Circuits and Systems for Video Technology* (Nov 2018), 3174–3182. doi:10.1109/tcsvt.2017.2740321
- [7] Chi-Min Chan, Weize Chen, Yusheng Su, Jianxuan Yu, Wei Xue, Shanghang Zhang, Jie Fu, and Zhiyuan Liu. 2023. ChatEval: Towards Better LLM-based Evaluators through Multi-Agent Debate. arXiv:2308.07201 [cs.CL] <https://arxiv.org/abs/2308.07201>
- [8] Jun Chen, Deyao Zhu, Xiaoqian Shen, Xiang Li, Zechun Liu, Pengchuan Zhang, Raghuraman Krishnamoorthi, Vikas Chandra, Yunyang Xiong, and Mohamed Elhoseiny. 2023. Minigt-v2: large language model as a unified interface for vision-language multi-task learning. arXiv preprint arXiv:2310.09478 (2023).
- [9] Wenliang Dai, Junnan Li, Dongxu Li, Anthony Meng Hua, Junqi Zhao, Weisheng Wang, Boyang Li, Pascale Fung, and Steven Hoi. [n. d.]. InstructBLIP: Towards General-purpose Vision-Language Models with Instruction Tuning. ([n. d.]).
- [10] Rohit Girdhar, Alaaeldin El-Nouby, Zhuang Liu, Mannat Singh, Kalyan Vasudev Alwala, Armand Joulin, and Ishan Misra. 2023. Imagebind: One embedding space to bind them all. In *Proceedings of the IEEE/CVF Conference on Computer Vision and Pattern Recognition*. 15180–15190.
- [11] Jiaming Han, Renrui Zhang, Wenqi Shao, Peng Gao, Peng Xu, Han Xiao, Kaipeng Zhang, Chris Liu, Song Wen, Ziyu Guo, et al. 2023. Imagebind-llm: Multi-modality instruction tuning. arXiv preprint arXiv:2309.03905 (2023).
- [12] Caner Hazirbas, Lingni Ma, Csaba Domokos, and Daniel Cremers. 2016. FuserNet: Incorporating depth into semantic segmentation via fusion-based cnn architecture. In *Asian conference on computer vision*. Springer, 213–228.
- [13] Xinxin Hu, Kailun Yang, Lei Fei, and Kaiwei Wang. 2019. Acnet: Attention based network to exploit complementary features for rgb-d semantic segmentation. In *2019 IEEE international conference on image processing (ICIP)*. IEEE, 1440–1444.
- [14] Jindong Jiang, Lunan Zheng, Fei Luo, and Zhijun Zhang. 2018. Rednet: Residual encoder-decoder network for indoor rgb-d semantic segmentation. arXiv preprint arXiv:1806.01054 (2018).
- [15] Katikapalli Subramanyam Kalyan. 2024. A survey of GPT-3 family large language models including ChatGPT and GPT-4. *Natural Language Processing Journal* 6 (2024), 100048.
- [16] Doyeon Kim, Woonghyun Ka, Pyungwhan Ahn, Donggyu Joo, Sehwan Chun, and Junmo Kim. 2022. Global-Local Path Networks for Monocular Depth Estimation with Vertical CutDepth. arXiv:2201.07436 [cs.CV] <https://arxiv.org/abs/2201.07436>
- [17] Junnan Li, Dongxu Li, Silvio Savarese, and Steven Hoi. 2023. BLIP-2: Bootstrapping Language-Image Pre-training with Frozen Image Encoders and Large Language Models. arXiv:2301.12597 [cs.CV] <https://arxiv.org/abs/2301.12597>
- [18] Junnan Li, Dongxu Li, Silvio Savarese, and Steven Hoi. 2023. Blip-2: Bootstrapping language-image pre-training with frozen image encoders and large language models. In *International conference on machine learning*. PMLR, 19730–19742.
- [19] Junnan Li, Dongxu Li, Caiming Xiong, and Steven Hoi. 2022. Blip: Bootstrapping language-image pre-training for unified vision-language understanding and generation. In *International conference on machine learning*. PMLR, 12888–12900.
- [20] KunChang Li, Yinan He, Yi Wang, Yizhuo Li, Wenhai Wang, Ping Luo, Yali Wang, Limin Wang, and Yu Qiao. 2023. Videochat: Chat-centric video understanding. arXiv preprint arXiv:2305.06355 (2023).
- [21] Ji Lin, Hongxu Yin, Wei Ping, Pavlo Molchanov, Mohammad Shoeybi, and Song Han. 2024. Vila: On pre-training for visual language models. In *Proceedings of the IEEE/CVF conference on computer vision and pattern recognition*. 26689–26699.
- [22] Tsung-Yi Lin, Michael Maire, Serge Belongie, Lubomir Bourdev, Ross Girshick, James Hays, Pietro Perona, Deva Ramanan, C. Lawrence Zitnick, and Piotr Dollár. 2015. Microsoft COCO: Common Objects in Context. arXiv:1405.0312 [cs.CV] <https://arxiv.org/abs/1405.0312>
- [23] Haotian Liu, Chunyuan Li, Yuheng Li, and Yong Jae Lee. 2024. Improved Baselines with Visual Instruction Tuning. arXiv:2310.03744 [cs.CV] <https://arxiv.org/abs/2310.03744>
- [24] Haotian Liu, Chunyuan Li, Qingyang Wu, and Yong Jae Lee. 2023. Visual Instruction Tuning. arXiv:2304.08485 [cs.CV] <https://arxiv.org/abs/2304.08485>
- [25] Zhiliang Peng, Wenhui Wang, Li Dong, Yaru Hao, Shaohan Huang, Shuming Ma, and Furu Wei. 2023. Kosmos-2: Grounding multimodal large language models to the world. arXiv preprint arXiv:2306.14824 (2023).
- [26] Alec Radford, Jong Wook Kim, Chris Hallacy, Aditya Ramesh, Gabriel Goh, Sandhini Agarwal, Girish Sastry, Amanda Askell, Pamela Mishkin, Jack Clark, Gretchen Krueger, and Ilya Sutskever. 2021. Learning Transferable Visual Models From Natural Language Supervision. arXiv:2103.00020 [cs.CV] <https://arxiv.org/abs/2103.00020>
- [27] Nathan Silberman, Derek Hoiem, Pushmeet Kohli, and Rob Fergus. 2012. Indoor segmentation and support inference from rgb-d images. In *Computer Vision—ECCV 2012: 12th European Conference on Computer Vision, Florence, Italy, October 7–13, 2012, Proceedings, Part V 12*. Springer, 746–760.
- [28] Shuran Song, Samuel P. Lichtenberg, and Jianxiong Xiao. 2015. SUN RGB-D: A RGB-D scene understanding benchmark suite. In *2015 IEEE Conference on Computer Vision and Pattern Recognition (CVPR)*. 567–576. doi:10.1109/CVPR.2015.7298655
- [29] Yixuan Su, Tian Lan, Huayang Li, Jialu Xu, Yan Wang, and Deng Cai. 2023. PandaGPT: One Model To Instruction-Follow Them All. arXiv:2305.16355 [cs.CL] <https://arxiv.org/abs/2305.16355>
- [30] Hugo Touvron, Thibaut Lavril, Gautier Izacard, Xavier Martinet, Marie-Anne Lachaux, Timothée Lacroix, Baptiste Rozière, Naman Goyal, Eric Hambro, Faisal Azhar, et al. 2023. Llama: Open and efficient foundation language models. arXiv preprint arXiv:2302.13971 (2023).
- [31] Hugo Touvron, Thibaut Lavril, Gautier Izacard, Xavier Martinet, Marie-Anne Lachaux, Timothée Lacroix, Baptiste Rozière, Naman Goyal, Eric Hambro, Faisal Azhar, Aurelien Rodriguez, Armand Joulin, Edouard Grave, and Guillaume Lample. 2023. LLaMA: Open and Efficient Foundation Language Models. arXiv:2302.13971 [cs.CL] <https://arxiv.org/abs/2302.13971>
- [32] Haoning Wu, Zicheng Zhang, Weixia Zhang, Chaofeng Chen, Liang Liao, Chunyi Li, Yixuan Gao, Annan Wang, Erli Zhang, Wenxiu Sun, Qiong Yan, Xiongkuo Min, Guangtao Zhai, and Weisi Lin. 2023. Q-Align: Teaching LLMs for Visual Scoring via Discrete Text-Defined Levels. arXiv:2312.17090 [cs.CV] <https://arxiv.org/abs/2312.17090>
- [33] Junjie Ye, Xuanting Chen, Nuo Xu, Can Zu, Zekai Shao, Shichun Liu, Yuhang Cui, Zeyang Zhou, Chao Gong, Yang Shen, Jie Zhou, Siming Chen, Tao Gui, Qi Zhang, and Xuanjing Huang. 2023. A Comprehensive Capability Analysis of GPT-3 and GPT-3.5 Series Models. arXiv:2303.10420 [cs.CL] <https://arxiv.org/abs/2303.10420>
- [34] Hang Zhang, Xin Li, and Lidong Bing. 2023. Video-llama: An instruction-tuned audio-visual language model for video understanding. arXiv preprint arXiv:2306.02858 (2023).
- [35] Bin Zhu, Bin Lin, Munan Ning, Yang Yan, Jiaxi Cui, HongFa Wang, Yatian Pang, Wenhao Jiang, Junwu Zhang, Zongwei Li, Wancai Zhang, Zhifeng Li, Wei Liu, and Li Yuan. 2024. LanguageBind: Extending Video-Language Pretraining to N-modality by Language-based Semantic Alignment. arXiv:2310.01852 [cs.CV] <https://arxiv.org/abs/2310.01852>
- [36] Deyao Zhu, Jun Chen, Xiaoqian Shen, Xiang Li, and Mohamed Elhoseiny. 2023. MiniGPT-4: Enhancing Vision-Language Understanding with Advanced Large Language Models. arXiv:2304.10592 [cs.CV] <https://arxiv.org/abs/2304.10592>